Exciton polariton including continuum states: Microscopic versus additional boundary conditions

E. A. Muljarov*
General Physics Institute, Russian Academy of Sciences, Vavilova 38, Moscow 119991, Russia

R. Zimmermann
Institut für Physik der Humboldt-Universität zu Berlin, Hausvogteiplatz 5-7, D-10117 Berlin, Germany
(Received 4 April 2002; revised manuscript received 29 August 2002; published 30 December 2002)

An exact method, based on microscopic boundary conditions, is developed for calculation of the optical properties of exciton polaritons with spatial dispersion. The method is formulated in a general manner for an arbitrary electron-hole potential and probed in the approximation of the one-dimensional contact interaction, in half-space and slab geometries. Another approach, based on approximate boundary conditions applied to all exciton bound and scattering states, generalizes the concept of additional boundary conditions. This approach yields analytical results for semi-infinite semiconductors and semiconductor slabs and allows us to extract and analyze the contribution of the exciton continuum states to the optical spectra of semiconductors. A correlation between reflectivity and transmission calculated in two different approaches demonstrates the crucial role of the strict boundary conditions in the correct computation of optical spectra.

DOI: 10.1103/PhysRevB.66.235319 PACS number(s): 71.36.+c, 78.20.Bh

I. INTRODUCTION

For more than 40 years the exciton polariton problem originally formulated by Pekar[1] and Hopfield[2] has been of permanent interest for intensive investigations[3–20] with a strong revival in recent years due to novel theoretical and experimental studies.[21–24]

In bulk semiconductors, the exciton center-of-mass and relative motions are decoupled, so that the exciton-photon interaction leaves unchanged the states of the excitonic hydrogen-like spectrum, on the one hand, and results in independent propagation of each polariton wave, on the other. This picture drastically changes as soon as one comes closer to the realistic situation, where the semiconductor surface influences the formation of excitonic states. Due to the break of translational symmetry at the interfaces, all bound and scattering exciton states are now mixed, and the macroscopic optical field in semiconductors is not only coupled to the ground state, but strongly influenced by higher bound states and especially by the excitonic continuum.

However, in early works[1–3,5–8] and in most recent papers (see, e.g., Refs. 17 and 24) the polariton problem has been treated in terms of $1S$ bulk excitons only, thus neglecting the contribution of all higher bound and scattering states. Within such a treatment one needs so-called additional boundary conditions (ABC's), since Maxwell's boundary conditions alone are insufficient to determine the amplitudes of two polariton waves propagating in the same direction.

Within the framework of the full microscopic approach, the correct microscopic boundary conditions (BC's) consist in a vanishing electron-hole amplitude on the semiconductor surfaces.[9] However, this exact solution of the polariton problem is an extremely complicated task and most of the microscopic approaches were based on additional assumptions and simplifications: (i) an analytical approximation of the exciton wave function neglecting the contribution of scattering states,[12] (ii) neglect of the electron-hole interaction,[14,20] (iii) neglect of the spatial dispersion[15] in the surface region, and so on. Only neglect of the recently have supercomputer abilities allowed one to attack the full problem by means of direct methods, solving a four-dimensional integro-differential material equation coupled with Maxwell's equation.[23] These calculations, however, have not been applied to frequencies above the band gap.

In the present paper we develop an approach to the exciton-polariton problem based on the microscopic framework[9,10] and strict BC's, expanding the electron-hole coherent amplitude into all bound and scattering exciton states. Here we present calculations for half-space and slab geometries in the simplest case of a one-dimensional (1D) contact potential, where most of the work can be done analytically. Further, results for semi-infinite semiconductors can be compared with existing calculations using another strict approach.[16] However, our method is formulated in quite a general manner and can be applied to realistic 3D Coulomb electron-hole interactions or to any other potential without too much additional complexities, compared to previous approaches.

In this work we also present a theory which generalizes the concept of ABC's. This concept introduced by Pekar[1] as macroscopic exciton polarization vanishing on the boundary $P=0$ (Pekar's ABC's) was later used by Ting, Frankel, and Birman[6] in the form of a zero slope of the polarization on the surface $P'=0$ (TFB ABC's) and by Kiselev *et al.*[7] in the mixed form $P'=\alpha P$, where α stands for a model parameter (mixed ABC's). In the literature, all kinds of ABC's were applied to the $1S$ excitonic polarization only. We explicitly include in the ABC theory the contribution of all other bound and continuum states. Our theory, based on the approximate center-of-mass BC's for the microscopic exciton polarization, yields exact analytical solutions (for half-space and slab) which show a much more realistic behavior of the reflectivity and transmission than the standard $1S$ ABC model (which is the special case of our result). The calculations can be improved significantly by adding a finite dead layer[3] wherein the exciton polarization vanishes. In particular, with the full 3D Coulomb dielectric function, it allowed us[25] to reproduce well-resolved oscillations far in the continuum in

the differential transmission of the high-quality 500-nm GaAs slab.[24]

Comparing results of calculations for the 1D contact potential obtained within strict and ABC models, we demonstrate the weak points of the latter, even improved by the inclusion of the Sommerefeld-enhanced continuum, and show the leading role of the exact BC's in an adequate description of the experimental results. At the same time we analyze the contribution of the exciton continuum states to the optical spectra and demonstrate its significance, especially at photon frequencies above the semiconductor band gap.

The paper is organized as follows. In Sec. II we develop an exact approach to the polariton problem in half-space and slab geometries; the details of the calculations are given in Appendixes A and B. Section III and Appendix C are devoted to the generalization of the ABC model to all bound and scattering states. In Sec. IV, in the example of the 1D contact electron-hole interaction, we analyze the contribution of the excitonic continuum as well as the strict BC's to the optical spectra of semi-infinite crystals and finite slabs and reevaluate the concept of the dead layer.

II. EXCITON POLARITON: STRICT APPROACH

Within the density matrix framework of the linear response theory and the two-band effective mass approximation, the exciton polariton problem in the case of normal incidence of light (the in-plane excitonic momenta $Q_x = Q_y = 0$) is described by the coupled material and Maxwell's equations[10]

$$\left[-\frac{\hbar^2}{2M}\frac{\partial^2}{\partial Z^2} + \hat{H}_{\rm ex}(\mathbf{r}) + E_g - \hbar\omega - i\gamma \right] Y(Z,\mathbf{r}) = \mathcal{M}\delta(\mathbf{r})E(Z), \tag{1}$$

$$\frac{\partial^2}{\partial Z^2}E(Z) + q_0^2\varepsilon_b E(Z) = -q_0^2\mathcal{M}Y(Z,0), \tag{2}$$

where $E(Z)$ is the electric field, $\tilde{Y}(\mathbf{r}_e,\mathbf{r}_h) = Y(Z,\mathbf{r})$ is the electron-hole coherent amplitude, $\mathcal{M}\delta(\mathbf{r})$ is the transition dipole density within the point dipole approximation, $\mathcal{M}Y(Z,0) = P(Z)$ is the macroscopic exciton polarization, $\hat{H}_{\rm ex}(\mathbf{r})$ is the Hamiltonian of the bulk exciton relative motion,

$$\hat{H}_{\rm ex}(\mathbf{r}) = -\frac{\hbar^2}{2\mu}\Delta_{\mathbf{r}} + V_{eh}(\mathbf{r}),$$

$V_{eh}(\mathbf{r})$ is the electron-hole potential, $\mathbf{r}$ and Z are, respectively, the relative and center-of-mass coordinates, $\mathbf{r} = \mathbf{r}_e - \mathbf{r}_h$, $Z = (m_e z_e + m_h z_h)/M$, $M = m_e + m_h$, $\mu = m_e m_h/M$, and $m_{e(h)}$ is the electron (hole) effective mass along z; $q_0 = \omega/c$, where ω is the photon frequency, γ is a phenomenological damping, E_g is the semiconductor gap energy, and ε_b is the background dielectric constant. In the following we assume an isotropic potential $V_{eh}(\mathbf{r})$. However, our approach can be easily generalized to any anisotropic interaction.

The full solution of Eqs. (1) and (2), $E(Z)$ and $Y(Z,\mathbf{r})$, should satisfy certain BC's. According to the Maxwell's BC's, both $E(Z)$ and $E'(Z)$ should be continuous everywhere. We assume an idealized infinite barrier at the semiconductor-vacuum interface, so that the correct BC's for the polarization should be its vanishing, if the electron or hole coordinate lies outside semiconductor,

$$\tilde{Y}(\mathbf{r}_e,\mathbf{r}_h) = 0,$$

$$\text{if} \quad z_e < 0,\ z_h < 0 \quad \text{(half space)},$$

$$\text{if} \quad z_e < 0,\ z_h < 0,\ z_e > L,\ z_h > L \quad \text{(slab)},$$

where L is the slab thickness, or in the relative and center-of-mass notation,

$$Y(Z_s(\mathbf{r}),\mathbf{r}) = 0, \tag{3}$$

where the function $Z_s(\mathbf{r})$ is properly defined below (see Secs. II A and II C). We have not included into Eq. (1) any surface potential, bearing in mind an abrupt boundary. We also neglect image potentials near semiconductor/vacuum or semiconductor/insulator interfaces because of its weak influence[26] on polariton properties, due to the exciton electroneutrality and quick (exponential) vanishing of the carrier wave functions in the vicinity of the interface.

A. Half-space geometry: Expansion into bulk eigenstates

In case of semi-infinite crystals the microscopic BC's Eq. (3), are applied on the semiconductor surface

$$Z_s(z) = \begin{cases} \dfrac{m_e}{M}z, & z > 0, \\ -\dfrac{m_h}{M}z, & z < 0. \end{cases} \tag{4}$$

Maxwell's BC's take the form (the amplitude of the incoming wave is taken to be unity)

$$E(0) + \frac{E'(0)}{iq_0} = 2, \tag{5}$$

where we assume a semiconductor/vacuum interface for simplicity. The reflection is described as follows:

$$r = E(0) - 1.$$

Let us expand the electric field and the electron-hole coherent amplitude into Fourier series

$$E(Z) = \sum_j E_j e^{ik_j Z}, \tag{6}$$

$$Y(Z,\mathbf{r}) = \sum_j Y_j(\mathbf{r}) e^{ik_j Z}, \tag{7}$$

where $\mathrm{Re}\,k_j > 0$ and $\mathrm{Im}\,k_j > 0$ due to decay and propagation conditions, explicitly related to each other due to finite γ.

Substituting Eqs. (6) and (7) into Eqs. (1) and (2) we obtain

$$\left[\frac{\hbar^2 k_j^2}{2M}+\hat{H}_{\rm ex}(\mathbf{r})+E_g-\hbar\omega-i\gamma\right]Y_j(\mathbf{r})=\mathcal{M}\delta(\mathbf{r})E_j, \quad (8)$$

$$E_j(-k_j^2+q_0^2\varepsilon_{\rm b})=-q_0^2\mathcal{M}Y_j(0). \quad (9)$$

We solve the system of equations (8) and (9) with the help of the bulk exciton one-coordinate Green's function which satisfies the following equation:

$$[\hat{H}_{\rm ex}(\mathbf{r})-\mathcal{E}]\tilde{G}(\mathcal{E};\mathbf{r})=\delta(\mathbf{r}),$$

with $\tilde{G}(\mathcal{E};\mathbf{r})\equiv\tilde{G}(\mathcal{E};\mathbf{r},\mathbf{r}'=0)$. The BC's for the Green's function are the absence of exponentially growing terms in $\tilde{G}$ at $\mathbf{r}\to\infty$. At the same time, $\tilde{G}$ has the asymptotic behavior

$$\tilde{G}(\mathcal{E};\mathbf{r})\propto e^{-\varkappa\mathbf{r}}, \quad \mathbf{r}\to\infty,$$

where

$$\varkappa=\sqrt{-\frac{2\mu}{\hbar^2}\mathcal{E}}=\sqrt{\frac{\mu}{M}k^2+\frac{2\mu}{\hbar^2}(E_g-\hbar\omega-i\gamma)}. \quad (10)$$

Then

$$\mathrm{Re}\,\varkappa\geqslant 0. \quad (11)$$

The presence of the square root, Eq. (10), in the Green's function means the existence of a cut in the complex k plane, starting from the point $\varkappa=0$ and going to infinity. As all k points of the cut contribute to the Fourier expansions Eqs. (6) and (7) (see below), the trajectory of the cut is unambiguously determined by the BC's for $\tilde{G}$ and Eq. (11) as follows:

$$\varkappa=\varkappa_c^{\pm}=\pm i\lambda, \quad 0\leqslant\lambda<\infty, \quad (12)$$

with the real parameter λ. Note that the ''plus'' or ''minus'' in Eq. (12) corresponds to different values of the Green's function (as well as $\varkappa$) defined on different sides of the cut. As $\mathcal{E}$ is one and the same for two different $\varkappa$'s, it is better to switch from $\mathcal{E}$ to $\varkappa$ in the argument of the Green's function, in order to distinguish its two different values on the cut,

$$G(\varkappa;\mathbf{r})\equiv\tilde{G}(\mathcal{E};\mathbf{r}).$$

After such an analysis we conclude that there are three possibilities for k_j contributing to Eqs. (6) and (7).

(i) Isolated poles k_p $(j=p)$ satisfying the dispersion relation of the bulk polariton,

$$k_p^2=q_0^2\varepsilon(k_p,\omega),$$

where the bulk exciton dielectric function $\varepsilon(k,\omega)$ is related to the Green's function in the standard way,

$$\varepsilon(k,\omega)=\varepsilon_{\rm b}+\mathcal{M}^2G(\varkappa;0); \quad (13)$$

$\varkappa(k,\omega)$ is given by Eq. (10). The solution takes the form

$$Y_p(\mathbf{r})=E_p\mathcal{M}G(\varkappa_p;\mathbf{r}). \quad (14)$$

(ii) Points on the cut $(j=c)$. The wave vector is determined by Eqs. (10) and (12) as follows:

$$k_c=\sqrt{\frac{2M}{\hbar^2}(\hbar\omega+i\gamma-E_g)-\frac{M}{\mu}\lambda^2}.$$

On the cut two different values of G correspond to one and the same E_c (and k_c). Thus, the solution of Eqs. (8) and (9) is a linear combination

$$Y_c(\mathbf{r})=E_c\mathcal{M}[\eta G(\varkappa_c^+;\mathbf{r})+(1-\eta)G(\varkappa_c^-;\mathbf{r})]. \quad (15)$$

Equation (9) now yields the condition for the coefficient η, instead of the dispersion relation.

(iii) Optically inactive (non-S) states $(j=\nu)$. For these states

$$E_\nu=Y_\nu(0)=0$$

and

$$Y_\nu(\mathbf{r})=C_\nu\varphi_\nu(\mathbf{r}), \quad (16)$$

where $\varphi_\nu(\mathbf{r})$ is the wave function of a non-S exciton state (bound or scattering) which satisfies the Schrödinger equation

$$\hat{H}_{\rm ex}(\mathbf{r})\varphi_\nu(\mathbf{r})=\mathcal{E}_\nu\varphi_\nu(\mathbf{r}). \quad (17)$$

The wave vector is again determined by Eq. (10) as follows:

$$k_\nu=\sqrt{\frac{2M}{\hbar^2}(\hbar\omega+i\gamma-E_g-\mathcal{E}_\nu)}. \quad (18)$$

Note that for the continuum non-S states the wave vector takes the same values as on the cut, $k_\nu=k_c$.

Finally, combining Eqs. (14), (15), and (16), the full electron-hole amplitude and the electric field have the form

$$Y(Z,\mathbf{r})=\sum_p E_p e^{ik_pZ}\mathcal{M}G(\varkappa_p;\mathbf{r}) + \int_{\rm cut}dk_cB(k_c)e^{ik_cZ}\mathcal{M}\left[\frac{G(\varkappa_c^+;\mathbf{r})}{D^+(k_c,\omega)}-\frac{G(\varkappa_c^-;\mathbf{r})}{D^-(k_c,\omega)}\right] + \sum\!\!\!\!\!\!\int_\nu C_\nu e^{ik_\nu Z}\varphi_\nu(\mathbf{r}), \quad (19)$$

$$E(Z)=\sum_p E_p e^{ik_pZ}+\int_{\rm cut}dk_cB(k_c)e^{ik_cZ}\left[\frac{1}{D^+(k_c,\omega)}-\frac{1}{D^-(k_c,\omega)}\right], \quad (20)$$

where

$$D^\pm(k_c,\omega)=q_0^2\varepsilon^\pm(k_c,\omega)-k_c^2, \quad (21)$$

and $\varepsilon^\pm$ is defined by Eq. (13) with $\varkappa=\varkappa_c^\pm$; E_c is renormalized to $B(k_c)$ for convenience [cf. Eqs. (15) and (19)].

B. Microscopic boundary conditions: Minimization of the exciton polarization on the boundary

In Sec. II A we have Fourier-expanded $Y(Z,\mathbf{r})$ and $E(Z)$, expressing the $\mathbf{r}$-dependent factors in Y in terms of bulk exciton eigenfunctions (for S states combined into the Green's function). However, the coefficients E_p, $B(k_c)$, and C_ν are still unknown and should be determined applying the BC's, Eqs. (3)–(5).

To satisfy the BC's, Eq. (3), let us require that $|Y(Z,\mathbf{r})|^2$ reach its minimum on the boundary $Z=Z_s(\mathbf{r})$. In other words, we minimize the form

$$\mathcal{W}=\int d\mathbf{r}|Y(Z_s(\mathbf{r}),\mathbf{r})|^2=(\vec{\xi},\hat{W}\vec{\xi}), \tag{22}$$

quadratic in

$$\vec{\xi}=\begin{bmatrix} E_p \\ B(k_c) \\ C_\nu \end{bmatrix}$$

and subjected to the additional condition

$$(\vec{\xi},\vec{a})=1, \tag{23}$$

resulting from Maxwell's BC's, Eq. (5). The scalar products in Eqs. (22) and (23) contain the necessary summation and integration, according to Eqs. (19) and (20), The integral operator $\hat{W}$ and the vector $\vec{a}$ are defined in Appendix A.

Finally, the minimum problem

$$\frac{\delta\mathcal{W}}{\delta\vec{\xi}}=0$$

with the condition Eq. (23) leads to the integral-matrix equation

$$\hat{W}\vec{\xi}=\sigma\vec{a}, \tag{24}$$

where σ is the Lagrange multiplier. The latter can be set to $\sigma=1$ in the first stage, the vector $\vec{\xi}$ being finally adjusted (by the proper factor) to the normalization condition, Eq. (23).

We have reduced the polariton problem to the first-order Fredholm equation (24) with the index of summation and integration running through the poles, the cut, and all non-S eigenstates of the bulk exciton. A similar but slightly modified procedure is applied to the slab geometry in Sec. II C (see below). Although Eq. (24) has a rather simple linear form, it may be prone to numerical instabilities and complete loss of information since the kernel is not diagonally dominated. By discretizing the continuous variables we convert the integral equation (24) into a matrix equation, which is subsequently solved via Gauss-Jordan elimination with pivoting (see, e.g., Ref. 27).

The integrated square modulus of the polarization mismatch minimized on the boundary, $\mathcal{W}_{\min}$, is plotted in Fig. 1 as a function of the excitation energy $\hbar\omega$. In order to check the relative accuracy, we have chosen to divide this value by the maximum of the amplitude $Y(Z,z)$ in the form $\max|Y(Z,z)|^2a_B^*$. The normalized quantity serves as a measure

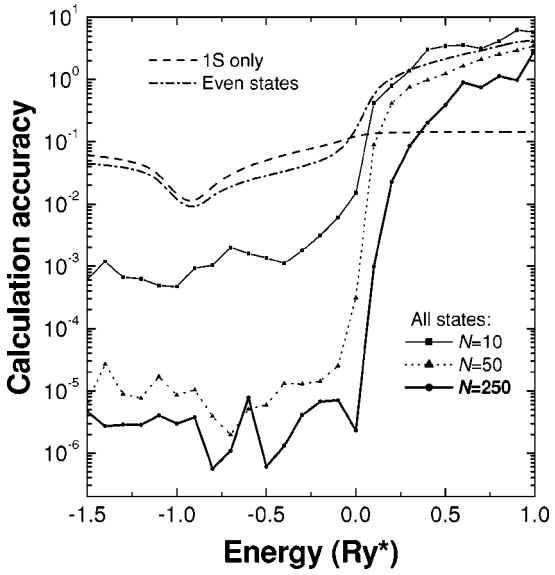

FIG. 1. $\mathcal{W}_{\min}$ divided by $\max|Y(Z,z)|^2a_B^*$, calculated for a semi-infinite crystal with parameters equal to bulk GaAs ($\gamma=0.05$ meV) with an account for only the 1S state (dashed curve), all even states (dash-dotted curve), and all bound and scattering states, using different numbers of discretization points in the continuum N (dotted and solid curves).

to which degree the boundary condition, Eq. (3), is fulfilled. The calculations are made within the 1D model with the contact electron-hole interaction (for details see Appendix B). At energies below the band gap, $\hbar\omega<E_g$ ($E<0$ in Fig. 1), the numerical solution of Eq. (24) is quite stable and does not depend on the number of discretization points in the continuum, N, for $N>50$ (cf. solid thick and dotted curves). At increasing energy, the solution becomes more and more unstable, so that a larger frequency requires a larger N to provide satisfactory accuracy. In fact, near the band gap $\mathcal{W}_{\min}$ grows suddenly, and convergency is not achieved even at the rather fine discretization of $N=250$ points. We believe that more sophisticated numerical algorithms could be devised which work in the continuum as well.

The minimization of the wave function on the boundary (in order to satisfy the microscopic BC's) has been already used in Ref. 11 for the 3D Coulomb half-space polariton problem. However, the contribution of the scattering states has been neglected there completely. As argued in Ref. 28, these contributions are expected to be of minor importance for CdS semi-infinite crystals. However, as seen from Fig. 1, in GaAs structures they play an important role. In fact, below the band gap, the dashed curve (bound states only) lies far above all other curves where the continuum is taken into account. Such a qualitative difference between CdS and GaAs parameters might be due to the larger exciton Bohr radius and the larger difference between electron and hole effective masses in GaAs. Above the band gap, the dashed curve finally crosses the solid thick curve, and the 1S approximation gives even better accuracy (still of the order of 20%) than our calculation including the continuum. This might be related to the above-mentioned convergency problems.

The dash-dotted curve in Fig. 1 is the result of a calculation which accounts for even states only, i.e., the sum over poles and the integral over the cut in Eq. (19). Surprisingly, the accuracy of this calculation turns out to be even worse than for 1*S* only. However, the comparison with the full calculation (solid thick curve) reveals another basic feature. Whereas in bulk semiconductors the non-*S* exciton states are optically inactive, in real systems with boundaries their role becomes crucial for optical properties. In fact, although non-*S* states do not appear in the expression for the electric field, Eq. (20), they contribute indirectly to $E(Z)$ through the BC's for $Y(Z,\mathbf{r})$. The latter, in turn, depends on E_p, $B(k_c)$, and C_ν and is minimized with respect to all of them simultaneously.

C. Slab geometry

Consider a semiconductor slab occupying the area $0 \leqslant Z \leqslant L$ (L is the slab thickness). The interface where the microscopic BC's, Eq. (3), should be satisfied now takes the form

$$Z_s(z)=\begin{cases} -\beta_h z \quad \text{or} \quad L+\beta_e z, \quad \text{if} \quad z<0, \\ \beta_e z \quad \text{or} \quad L-\beta_h z, \quad \text{if} \quad z>0, \end{cases} \tag{25}$$

where $\beta_{e,h}=m_{e,h}/M$. Compared to semi-infinite crystals, there are both copropagating and contrapropagating waves in the slab. The simplest way to solve the slab problem is to divide the electric field and polarization inside the slab into even and odd parts,

$$E(Z)=E_e(Z)+E_o(Z),$$

$$Y(Z,\mathbf{r})=Y_e(Z,\mathbf{r})+Y_o(Z,\mathbf{r}),$$

and to apply the procedure described in Secs. II A and II B to even and odd problems separately. As follows from the symmetry properties,

$$E_{e,o}(Z)=sE_{e,o}(L-Z),$$

$$Y_{e,o}(Z,\mathbf{r})=sY_{e,o}(L-Z,-\mathbf{r}),$$

where

$$s=\begin{cases} +1, & \text{even}, \\ -1, & \text{odd}. \end{cases} \tag{26}$$

The expressions for Y and E take the form

$$\begin{aligned} Y_{e,o}(Z,\mathbf{r})=&\sum_p E_p[e^{ik_pZ}+se^{ik_p(L-Z)}]\mathcal{M}G(\varkappa_p;\mathbf{r}) \\ &+\int_{\text{cut}} dk_c B(k_c)[e^{ik_cZ} \\ &+se^{ik_c(L-Z)}]\mathcal{M}\left[\frac{G(\varkappa_c^+;\mathbf{r})}{D^+(k_c,\omega)}-\frac{G(\varkappa_c^-;\mathbf{r})}{D^-(k_c,\omega)}\right] \\ &+\sum\!\!\!\!\!\!\int_\nu C_\nu[e^{ik_\nu Z}-se^{ik_\nu(L-Z)}]\varphi_\nu(\mathbf{r}), \end{aligned} \tag{27}$$

$$\begin{aligned} E_{e,o}(Z)=&\sum_p E_p[e^{ik_pZ}+se^{ik_p(L-Z)}]+\int_{\text{cut}} dk_c B(k_c)[e^{ik_cZ} \\ &+se^{ik_c(L-Z)}]\left[\frac{1}{D^+(k_c,\omega)}-\frac{1}{D^-(k_c,\omega)}\right]. \end{aligned} \tag{28}$$

If the slab is surrounded by vacuum on both sides, Mawxell's BC's have the form [cf. with Eq. (5)]

$$E_{e,o}(0)+\frac{E'_{e,o}(0)}{iq_0}=1, \tag{29}$$

the reflection and transmission being described as

$$r=E_e(0)+E_o(0)-1,$$

$$t=E_e(0)-E_o(0).$$

The matrix elements of $\hat{W}$ can be found in the same way as in half-space geometry. Their analytical expressions are given in Appendix B for the special case of the 1D contact potential, calculated for both half-space and slab geometries.

III. ABC MODEL

In this section we develop an approach based on the approximate center-of-mass (c.o.m.) boundary condition instead of the exact one: The function $Z_s(\mathbf{r})$ in Eq. (3) is assumed to be $\mathbf{r}$ independent. At first glance, this approximation is equivalent to the ABC's introduced by Pekar,[1] namely $P=0$, where P is the macroscopic polarization. However, in our approach this condition is applied not only to the ground state of the bulk exciton, as it is usually used, but to all parts of polarization produced by bound and scattering states.

Let us expand the electron-hole coherent amplitude into bulk exciton states

$$Y(Z,\mathbf{r})=\sqrt{\frac{2M}{\hbar^2}}\sum\!\!\!\!\!\!\int_\nu P_\nu(Z)\varphi_\nu(\mathbf{r}), \tag{30}$$

where the eigenfunctions $\varphi_\nu(\mathbf{r})$ satisfy Eq. (17) and constitute a complete set; ν takes all possible quantum numbers of both *S* and non-*S* states. From Eqs. (1) and (2) we get

$$P''_\nu(Z)+k_\nu^2 P_\nu(Z)=-\mathcal{M}_\nu^* E(Z), \tag{31}$$

$$E''(Z)+q_0^2\varepsilon_b E(Z)=-q_0^2\sum\!\!\!\!\!\!\int_\nu \mathcal{M}_\nu P_\nu(Z), \tag{32}$$

where

$$\mathcal{M}_\nu=\sqrt{\frac{2M}{\hbar^2}}\varphi_\nu(0)\mathcal{M},$$

and k_ν is given by Eq. (18).

The BC's for the c.o.m. motion take the form

$$Y(Z_s,\mathbf{r})=0. \tag{33}$$

As Z_s does not depend on $\mathbf{r}$, Eq. (33) can be satisfied only if

$$P_\nu(Z_s)=0 \tag{34}$$

for each ν. In other words, it is assumed that the polariton c.o.m. and relative motions are decoupled on the boundary.

One should note that the non-S states [with $\mathcal{M}_\nu=\varphi_\nu(0)=0$] do not produce the macroscopic polarization $P(Z)=\mathcal{M}Y(Z,0)$ and thus are neglected in the present model. On the other hand, as is shown in Sec. II, even in the strict approach, the contribution of S states can be combined into the Green's function; see Eqs. (19) and (20). Thus, it is expected (and we show it below) that the final results depend only on the bulk exciton dielectric function, Eq. (13), all the material information being concentrated in.

First, we consider a semiconductor slab and derive the exciton polarization, expanding it into slab eigenmodes. The expressions for half-space geometry follow automatically as a limiting case of infinitely wide slab.

A. Slab geometry

For a semiconductor slab, occupying the area $0\leqslant Z\leqslant L$, the BC's, Eq. (34), read

$$P_\nu(0)=P_\nu(L)=0. \tag{35}$$

Let us expand $P_\nu(Z)$ into slab eigenmodes as

$$P_\nu(Z)=\sum_n P_{\nu n}u_n(Z), \tag{36}$$

where the orthonormal functions

$$u_n(Z)=\frac{2i\sin(k_nZ)}{\sqrt{2L}},\quad k_n=\frac{\pi n}{L},\quad n=1,2,\ldots,$$

satisfy the differential equation

$$u_n''(Z)+k_n^2u_n(Z)=0,$$

the same boundary conditions as Eq. (35), $u_n(0)=u_n(L)=0$, and thus constitute a complete set for the class of functions specified by Eq. (35). Being a solution of inhomogeneous differential equation (32), the electric field can be expressed as a superposition of homogeneous and inhomogeneous parts,

$$E(Z)=A_+e^{iq_1Z}+A_-e^{-iq_1Z}+\sum_n E_n^{\mathrm{inh}}u_n(Z),\quad q_1=q_0\sqrt{\varepsilon_b}, \tag{37}$$

with the inhomogeneous part also satisfying Eq. (35), whereas the coefficients $A_\pm$ of the homogeneous part are fixed by Maxwell's BC's. From Eqs. (31) and (32) we get

$$E_n^{\mathrm{inh}}=-\frac{q_0^2}{q_0^2\varepsilon_b-k_n^2}\sum_\nu \mathcal{M}_\nu P_{\nu n}, \tag{38}$$

$$P_{\nu n}=-\frac{\mathcal{M}_\nu^*}{k_\nu^2-k_n^2}(E_n^{\mathrm{hom}}+E_n^{\mathrm{inh}}), \tag{39}$$

where the coefficients of the homogeneous part are formally defined as

$$E_n^{\mathrm{hom}}=\int_0^L(A_+e^{iq_1Z}+A_-e^{-iq_1Z})u_n^*(Z)dZ. \tag{40}$$

On the boundaries we have

$$E(0)=A_++A_-,$$

$$E(L)=A_+e^{iq_1L}+A_-e^{-iq_1L}. \tag{41}$$

Finally, combining Eqs. (38)–(41) and taking into account the fact that

$$\varepsilon(k,\omega)=\varepsilon_b+\sum_\nu \frac{|\mathcal{M}_\nu|^2}{k^2-k_\nu^2}$$

[cf. with Eq. (13)], we arrive at

$$E(Z)=\frac{i}{L}\sum_{n=-\infty}^{\infty}\frac{E(0)-(-1)^nE(L)}{q_0^2\varepsilon(k_n,\omega)-k_n^2}k_ne^{ik_nZ}. \tag{42}$$

The series in Eq. (42) describes the electric field within the slab. It converges everywhere except $Z=0$ and $Z=L$, where the equation should give identity and thus is practically useless. To complete the use of Maxwell's BC's and to calculate reflection and transmission one should also consider E' on the boundaries. Taking the derivative of Eq. (42) and using a regularization procedure (see Appendix C), we obtain

$$E'(Z)=-\frac{1}{L}\sum_{n=-\infty}^{\infty}[E(0)-(-1)^nE(L)]\times\frac{q_0^2\varepsilon(k_n,\omega)}{q_0^2\varepsilon(k_n,\omega)-k_n^2}e^{ik_nZ},$$

where the series is now convergent both inside the interval $0<Z<L$ and on the boundaries $Z=0$ and $Z=L$.

B. Half-space geometry

Treating the half-space problem as a limiting case of an extremely wide slab $L\to\infty$ and switching to integrals $\Sigma_n\to(L/\pi)\int dk$, we deduce from Eq. (42)

$$E(Z)=\int_{-\infty}^{\infty}dk\frac{B(k)e^{ikZ}}{q_0^2\varepsilon(k,\omega)-k^2}, \tag{43}$$

with

$$B(k)=\frac{i}{\pi}E(0)k. \tag{44}$$

In Appendix C we consider a more general case of mixed ABC's, Eq. (C1), which, compared to Pekar's ABC's, Eq. (33), contains both P and P', connected via the model parameter α. If $\alpha\to\infty$, Eq. (C1) reproduces Pekar's ABC's,

whereas $\alpha=0$ results in ABC's, suggested by Ting, Frankel, and Birman[6] and, being applied to all bound and scattering states, yields Eq. (43) with

$$B(k)=\frac{1}{\pi}E'(0).$$

This result exactly coincides with that obtained in recent paper by Henneberger[21] on the basis of an *ad hoc* assumption that the nonlocal part of the exciton polarization is localized within a thin surface layer, so that the inhomogeneous current on the boundary can be approximated by a δ function. It can be shown, however, that in most semiconductors the thickness of the surface layer is of the order of the exciton Bohr radius a_B^* (see also Sec. IV), so that the long-wavelength limit $ka_B^*\ll 1$ assumed in Ref. 21 cannot be fulfilled. Moreover, the model of two independent δ layers on the boundaries, $\delta(Z)$ and $\delta(Z-L)$, proposed in Ref. 21 for calculation of the electric field in a slab means in reality no correlations between the boundaries and gives a result completely different from Eqs. (42) and (C6), where the infinite sum has the physical meaning of multiple reflections of polariton waves from the interfaces.

C. Comparison with the strict method

Although the strict and ABC approaches are based on different BC's, the results, Eq. (20) and Eq. (43), are closely correlated. In fact, the poles k_p in Eq. (20) are the solutions of

$$D(k,\omega)=0,$$

where $D(k,\omega)$ is defined by Eq. (21) and coincides with the denominator of the integrand in Eq. (43). Further, the integral along the real axis k in Eq. (43) can be transformed into a sum of residua at $k=k_p$ with

$$\frac{2\pi i B(k_p)}{D_k'(k_p,\omega)}=E_p$$

and the integral along a contour surrounding the cut, the latter being equal to the integral in Eq. (20). The same thing can be done with the polarization $P(Z)$. Thus, we bring the expressions for $E(Z)$ and $P(Z)$ obtained in two different models to one and the same form. Obviously, $B(k)$ is different in two approaches. Also, it has the analytical form, Eq. (44), in the ABC model, whereas in the exact treatment it is found numerically from the matrix equation (24). However, the case of Pekar's ABC's, Eq. (44) can be also reproduced within the strict method, setting in the model assumption

$$\beta_e=\beta_h=0,$$

which means a nonrealistic condition of $m_e=m_h=0$ together with finite M and μ at the same time.

We would like to note that the most explicit disadvantage of the ABC model is the neglect of non-S states, which follows automatically from the approximate BC's. It is known, however, that the contribution of these states to the optical properties of real systems is very important. For instance, in semi-infinite semiconductors, in the limit of $M\to\infty$, the exciton wave function of the ground state is purely of P type strictly on the boundary.[29] The importance of the non-S states is also confirmed by our calculations based on the exact theory of Sec. II.

IV. RESULTS AND DISCUSSIONS

The two different approaches developed in Secs. II and III are tested with the help of a simple 1D model with the electron-hole interaction of contact type. Within such a model, the Green's function and the matrix elements appearing in the strict approach can be derived analytically (see Appendix B). Corresponding results for the 3D Coulomb interaction within the ABC model have been published elsewhere.[25]

The dielectric function, Eq. (13), which is the essential building block in both approaches, depends on two material parameters, the background dielectric constant $\tilde{\varepsilon}_b$ and the longitudinal-transverse splitting $\tilde{\Delta}_{\mathrm{LT}}$ (proportional to $\mathcal{M}^2$). Being effective adjustable parameters, they depend on how many states are taken in the bulk exciton susceptibility, since they have to account for the the contribution of the rest which is not treated explicitly. We relate these parameters to the measured quantities ε_b and Δ_{LT} using the following conditions:

$$\mathrm{Re}[\varepsilon(0,\omega_t+i\gamma/\hbar)]=\varepsilon_b,$$

$$\mathrm{Re}[\varepsilon(0,\omega_t+\Delta_{\mathrm{LT}}/\hbar)]=0,$$

where $\hbar\omega_t$ is the (transverse) exciton $1S$ energy.

The calculations of reflectivity and transmission are done for finite slabs and the semi-infinite case with parameters of bulk GaAs: $\varepsilon_b=12.66$, $\Delta_{\mathrm{LT}}=0.086$ meV, $E_g=1519.0$ meV, $\hbar\omega_t=1514.8$ meV, $m_e=0.0667m_0$, $m_h=0.45m_0$, and $\gamma=0.05$ meV.

For half-space geometry we have found an excellent agreement with the results by Victor *et al.*,[16] where specific properties of the 1D contact potential together with the point-dipole approximation led to substantial simplifications in the analytical part of their approach. However, the method of Ref. 16 turns out to be extremely hard when applied to the slab geometry and is practically impossible for the realistic 3D Coulomb electron-hole interaction.

Figure 2 shows the polarization amplitude $|P(Z)|=\mathcal{M}|Y(Z,0)|$ in a semi-infinite crystal, calculated within the strict approach and the ABC model with Pekar's BC's (thick and thin curves, respectively), for different frequencies of the external electromagnetic field.[30] In order to compare the results of both approaches we have chosen to shift the Pekar polarization by a proper distance Δl which lines up approximately the maxima and minima in both curves. This is at the heart of the exciton dead-layer concept proposed by Hopfield and Thomas[3] and used in several succeeding papers. Further, we introduce into this model a new adjustable parameter, which is the dielectric constant of the dead layer $\varepsilon_{\Delta l}$. This parameter effectively accounts for some finite contribution of

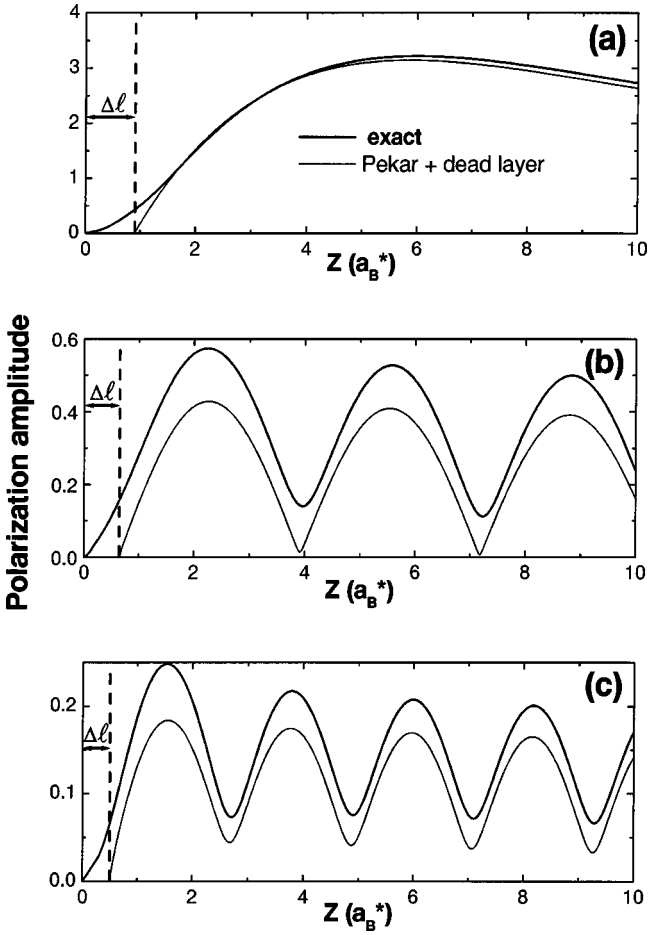

FIG. 2. Polarization amplitude $|P(Z)|$ of a semi-infinite crystal, calculated in exact (thick curves) and ABC (thin curves) approaches. The amplitude of the electric field in the incident beam is taken to be unity. The photon energy and the dead-layer thickness are, respectively, (a) $\hbar\omega - E_g = -\mathrm{Ry}^*$, $\Delta l = 0.9 a_B^*$; (b) $\hbar\omega - E_g = -0.5$ Ry*, $\Delta l = 0.65 a_B^*$; (c) $\hbar\omega - E_g = 0$, $\Delta l = 0.5 a_B^*$.

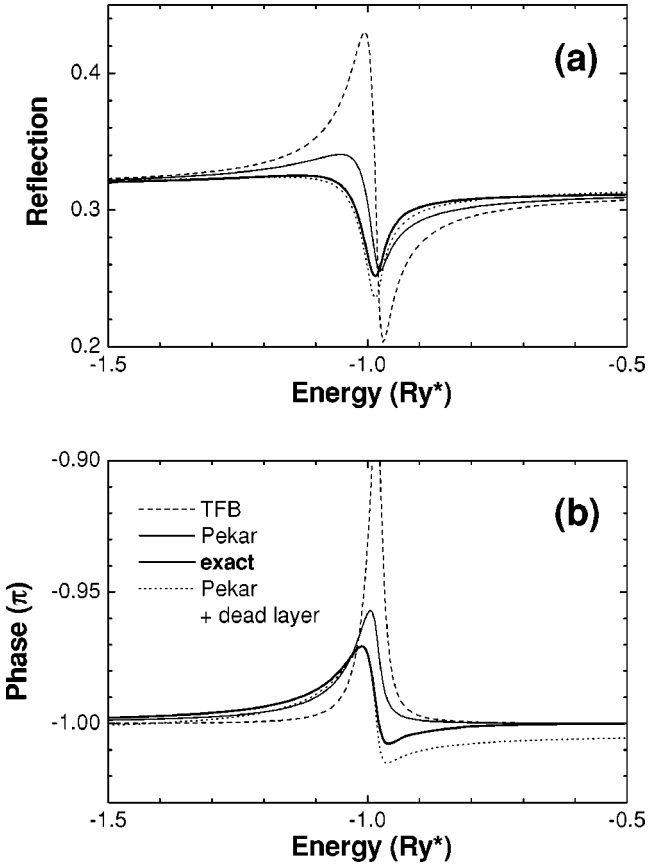

FIG. 3. Reflectivity $|r|^2$ (a) and phase $\arg(r)$ (b) of a semi-infinite crystal, calculated within the 1D contact potential with parameters equal to bulk GaAs (see the text), in the exact approach (thick curves) and in ABC models: Pekar (solid curves), TFB (dashed curves), and Pekar with dead layer (dotted curves). The parameters of the dead layer are taken as $\Delta l = 0.85 a_B^*$, $\varepsilon_{\Delta l} = 13.5$. The photon energy is measured in Ry*.

the actual exciton polarization within this layer and should be, in principle, larger than the background dielectric constant ε_b.

As seen from the polarization plots in Fig. 2, Pekar's ABC's, even augmented by a dead layer, give only qualitative agreement with the exact result. Moreover, the dead-layer thickness Δl has to depend on frequency. The reason is that the oscillations in the polarization originate from the mismatch between the resonant exciton and the photon energies. The oscillation frequency vanishes at $\omega = \omega_t$ [panel (a)] and grows with the detuning $\omega - \omega_t$ [panels (b) and (c)]. Consequently, Δl decreases as the frequency of the exciton-photon beating increases. Note, however, that within a sizable frequency region around the exciton resonance, Δl is of the order of the exciton effective Bohr radius a_B^* and characterizes the depth of polarization inhomogeneity near the semiconductor surface. As soon as Δl is small (due to parameters of a particular semiconductor) compared to the characteristic length where the polarization changes significantly, $a_B^* \ll (\sqrt{\varepsilon_b}\omega/c)^{-1}$, the difference between the Pekar and exact polarizations becomes unimportant and the use of the Pekar ABC model is justified.

Having introduced the mixed ABC model governed by the mixing constant α (Appendix C), we have studied the behavior of the optical response for any complex α.[31] We found that among all ABC's, Pekar's ABC's give results which are closest to the exact ones (cf. thin and thick solid curves in Fig. 3), whereas TFB (Henneberger's) ABC's (Fig. 3, dashed curves) lead to reflectivity and phase spectra which are close to the limit $M \to \infty$, i.e., without spatial dispersion. At the same time, the TFB spectra deviate strongly from the exact ones. Mixed ABC's with finite α give either results somewhere between Pekar's and TFB ABC's or turn out to be completely unrealistic.

Looking closer we have to ascertain that in half-space geometry, Pekar's ABC's give an optical response which is still far from the exact one. Even with the improvement of a dead layer (dotted curves), there is no way to match *reflectivity and phase simultaneously* with the exact results, in agreement with the findings in Ref. 23. We conclude that no ABC can give fully satisfactory results, and the strict microscopic BC's should be used for an adequate description of

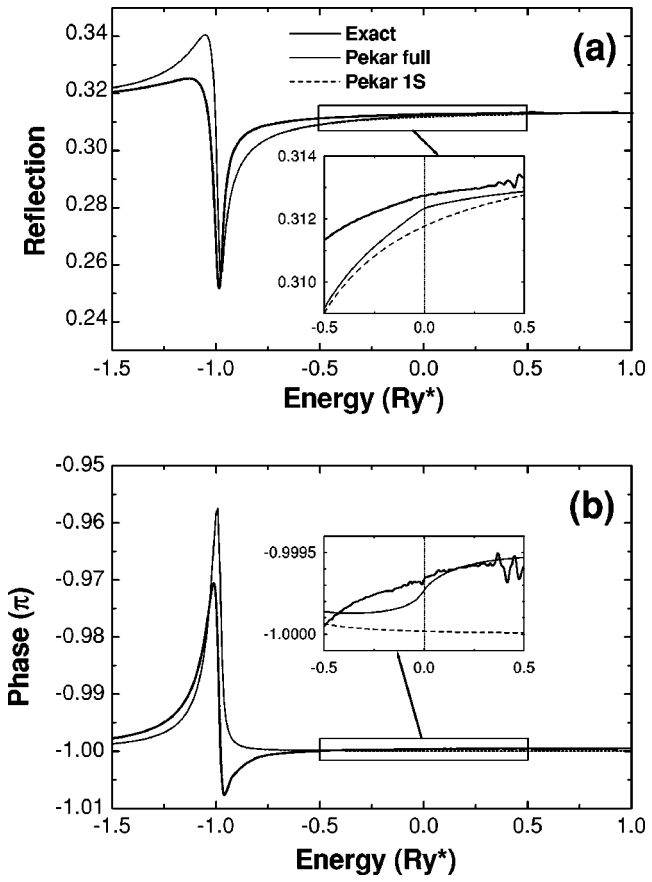

FIG. 4. The same as in Fig. 2, calculated in the exact approach (thick curves) and in Pekar's ABC model with (solid curves) and without scattering states (dashed curves).

polaritons and their optical properties in bounded semiconductors.

To analyze the influence of the continuum we plot in Fig. 4 reflectivity and phase calculated within the exact approach and Pekar's ABC's, with and without a continuum (no dead layer). The 1D contact potential has only one bound state ($1S$ exciton state), being energetically well separated from the continuum onset, which reduces the importance of the scattering states.[32] However, Pekar's ABC's applied to all states or to $1S$ only lead to qualitatively different results (the difference is quite visible in the inset to Fig. 4, solid and dashed curves): Near the continuum onset, the scattering states cause a break in slope, in particular in reflection [panel (a)], whereas the $1S$ curves are completely smooth. This break, however, is an artifact and does not appear in the exact calculation (thick curves), which accounts properly for the scattering states.

As we have already mentioned, our numerical scheme is not well converged at energies above 0.5 Ry* (see the inset to Fig. 4). This calls for more sophisticated numerical methods to solve Eq. (24) than used in the present work. However, note that in the calculations, we have taken an extremely small broadening $\gamma=0.05$ meV, being approximately 1% of the effective Rydberg. Larger broadening moves the convergence limit further into the continuum, with a significant improvement of the results. For a slab calculation, however, this tends to wash out any structure in the continuum. Recent experiments[24] on high-quality GaAs samples have shown very-well-resolved oscillations in differential transmission way up in the continuum. This implies a rather small homogeneous damping.

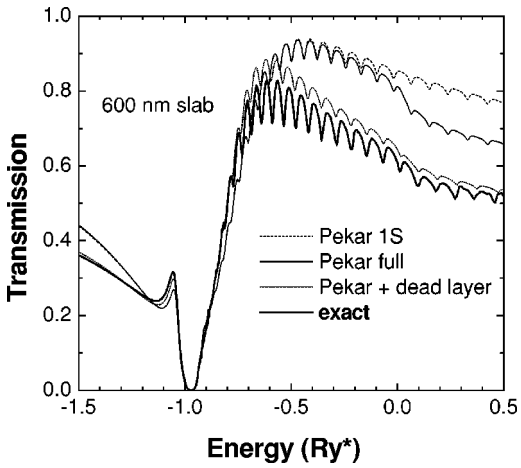

FIG. 5. Transmission $|t|^2$ of a 600 nm slab calculated within the 1D contact potential with parameters equal to bulk GaAs, in the exact approach (thick curve) and in Pekar's ABC model with (solid and dotted curves) and without (dashed curve) scattering states. The parameters of the dead layer are taken as $\Delta l=5$ nm, $\varepsilon_{\Delta l}=18.5$. The photon energy is measured in Ry*.

Transmission spectra of a 600 nm slab calculated with bulk GaAs parameters are displayed in Fig. 5. The most characteristic features in the polariton spectra of a slab are the oscillations due to the quantization of the exciton center-of-mass motion.[8,14,17] Qualitatively, the transmission is expected to have structures at the energies

$$E_n=\hbar\omega_t+\frac{\hbar^2\pi^2n^2}{2ML^2}, \tag{45}$$

which describe the slab quantization of the $Q_x=Q_y=0$ exciton, neglecting its relative motion. As follows from the analytical form of the electric field in a slab, Eq. (42), calculated with Pekar's ABC's, the maxima and minima of $E(Z)$ are expected near the frequencies ω satisfying

$$\varepsilon(k_n,\omega)=0.$$

Neglecting the contribution of all exciton states other than $1S$ leads to $\hbar\omega=E_n$ from Eq. (45). However, the transmission maxima or minima do not follow strictly Eq. (45), even in the $1S$-only Pekar model, but dipslay systematic shifts.

As a rule, the discrepancies between the different models are more striking in the slab geometry and especially in the continuum. Compared to the half-space geometry, the Pekar transmission spectra calculated with and without scattering states significantly differ from each other above the band gap (cf. solid and dashed curves in Fig. 5). Both curves, however, deviate strongly from the exact one (thick curve). Only the inclusion of a 5 nm dead layer with $\varepsilon_{\Delta l}=18.5$ (much larger than in half-space) into Pekar's ABC model (Fig. 5, dotted curve) gives reasonable agreement with the exact results,

both in overall slope and positions of extrema. Nevertheless, the oscillation amplitude is a factor of 2.5 too small, and the detailed shape is still unsatisfactory. We would like to stress that the TFB ABC's and Henneberger's model (being completely different in the slab geometry) fail to give any oscillations in the transmission for any reasonable nonzero γ.

V. CONCLUSIONS

We have developed an exact method which allows one to calculate reflection and transmission spectra of exciton polaritons. The microscopic boundary conditions have been converted into a minimization problem leading to an integral-matrix equation. Within the 1D contact potential, the kernel could be derived analytically, and the subsequent numerical solution was possible. This method can be applied, without too much effort, to the Coulomb or any other potential, and including an anisotropic kinetic energy.

On the basis of approximate boundary conditions applied to the exciton center-of-mass motion, we have generalized the ABC model to include all bound and scattering states, and have obtained analytical results for half-space and slab geometries. The model has been extended to the general situation of mixed ABC's.

We have shown that the calculations within the ABC's and the exact approach lead to results which differ in principle. The inclusion of an exciton dead layer into the ABC model is an improvement. However, serious discrepancies still remain between exact and ABC spectra, such as different oscillation amplitudes in the slab transmission or different background values in the half-space reflectivity. Moreover, two adjustable parameters, the dead-layer thickness and its dielectric constant, have to be added to the ABC model. These additional parameters are usually unknown and frequency dependent. Thus, for a correct evaluation of the polariton optical spectra it is necessary to account for the exact microscopic boundary conditions.

In both approaches the continuum states of the excitonic spectrum contribute to the microscopic polarization in an explicit way. Analyzing the fraction of the continuum in the excitonic polarization, we have demonstrated its significant role in the optical properties, especially above the semiconductor band edge.

ACKNOWLEDGMENTS

One of us (E.A.M.) has been supported by Deutscher Akademischer Austauschdienst (NATO Grant No. 325-A/99/02854), INTAS (Grant No. YSF 00-40), and in part by the Russian Foundation for Basic Research and by the Russian Ministry of Science. The authors are thankful to A. Stahl, G. Göger, K. Henneberger, and S. G. Tikhodeev for useful discussions.

APPENDIX A: MINIMIZATION OF THE EXCITONIC POLARIZATION ON THE SEMICONDUCTOR BOUNDARY

To satisfy the boundary conditions (3) let us minimize the following form, quadratic in E_p, $B(k_c)$, and C_ν:

$$\mathcal{W}=\sum_{p,p'} E_p^*\mathcal{W}_{11}(k_p,k_{p'})E_{p'}+\sum_p \int_{\rm cut} dk_{c'}E_p^*\mathcal{W}_{12}(k_p,k_{c'})B(k_{c'})+\sum_p \sum\!\!\!\!\!\!\int_{\nu'} E_p^*\mathcal{W}_{13}(k_p,k_{\nu'})C_{\nu'}$$
$$+\int_{\rm cut} dk_c \sum_{p'} B^*(k_c)\mathcal{W}_{21}(k_c,k_{p'})E_{p'}+\int_{\rm cut} dk_c\int_{\rm cut} dk_{c'}B^*(k_c)\mathcal{W}_{22}(k_c,k_{c'})B(k_{c'})+\int_{\rm cut} dk_c \sum\!\!\!\!\!\!\int_{\nu'} B^*(k_c)\mathcal{W}_{23}(k_p,k_{\nu'})C_{\nu'}$$
$$+\sum\!\!\!\!\!\!\int_{\nu}\sum_{p'} C_\nu^*\mathcal{W}_{31}(k_\nu,k_{p'})E_{p'}+\sum\!\!\!\!\!\!\int_{\nu}\int_{\rm cut} dk_{c'}C_\nu^*\mathcal{W}_{32}(k_\nu,k_{c'})B(k_{c'})+\sum\!\!\!\!\!\!\int_{\nu}\sum\!\!\!\!\!\!\int_{\nu'} C_\nu^*\mathcal{W}_{33}(k_\nu,k_{\nu'})C_{\nu'}, \tag{A1}$$

where

$$\mathcal{W}_{11}(k_p,k_{p'})=V_{00}(\varkappa_p,\varkappa_{p'}),$$

$$\mathcal{W}_{12}(k_p,k_{c'})=\frac{V_{00}(\varkappa_p,i\lambda')}{D^+(k_{c'})}-\frac{V_{00}(\varkappa_p,-i\lambda')}{D^-(k_{c'})},$$

$$\mathcal{W}_{22}(k_c,k_{c'})=\frac{V_{00}(i\lambda,i\lambda')}{D^{+*}(k_c)D^+(k_{c'})}-\frac{V_{00}(i\lambda,-i\lambda')}{D^{+*}(k_c)D^-(k_{c'})}$$
$$-\frac{V_{00}(-i\lambda,i\lambda')}{D^{-*}(k_c)D^+(k_{c'})}+\frac{V_{00}(-i\lambda,-i\lambda')}{D^{-*}(k_c)D^-(k_{c'})},$$

$$\mathcal{W}_{13}(k_p,k_{\nu'})=V_{01}(\varkappa_p,\varkappa_{\nu'}),$$

$$\mathcal{W}_{23}(k_c,k_{\nu'})=\frac{V_{01}(i\lambda,\varkappa_{\nu'})}{D^{+*}(k_c)}-\frac{V_{01}(-i\lambda,\varkappa_{\nu'})}{D^{+*}(k_c)},$$

$$\mathcal{W}_{33}(k_\nu,k_{\nu'})=V_{11}(\varkappa_\nu,\varkappa_{\nu'}),$$

$$\mathcal{W}_{ji}(k_2,k_1)=\mathcal{W}^*_{ij}(k_1,k_2). \tag{A2}$$

For the half-space problem the matrix elements have the form

$$V_{00}(\varkappa_1,\varkappa_2)=\mathcal{M}^2\int d\mathbf{r}\,G^*(\varkappa_1;\mathbf{r})G(\varkappa_2;\mathbf{r})e^{-i(k_1^*-k_2)Z_s(z)},$$

$$V_{01}(\varkappa,\varkappa_\nu)=\mathcal{M}\int d\mathbf{r}\,G^*(\varkappa;\mathbf{r})\varphi_\nu(\mathbf{r})e^{-i(k^*-k_\nu)Z_s(z)},$$

$$V_{11}(\varkappa_\nu,\varkappa_{\nu'})=\int d\mathbf{r}\,\varphi^*_\nu(\mathbf{r})\varphi_{\nu'}(\mathbf{r})e^{-i(k^*_\nu-k_{\nu'})Z_s(z)}, \tag{A3}$$

where

$$k=\sqrt{\frac{2M}{\hbar^2}(\hbar\omega+i\gamma-E_g)+\frac{M}{\mu}\varkappa^2}, \tag{A4}$$

$$\varkappa_\nu=\sqrt{-\frac{2\mu\mathcal{E}_\nu}{\hbar^2}}.$$

Maxwell's BC's yield

$$\sum_p\frac{1+k_p/q_0}{2}E_p+\int_{\text{cut}}dk_c\frac{1+k_c/q_0}{2}\left[\frac{1}{D^+(k_c)}-\frac{1}{D^-(k_c)}\right]B(k_c)=1. \tag{A5}$$

The minimum problem results in Eq. (24), where the operator $\hat{W}$ has the matrix elements, Eq. (A2), and contains necessary summations and integrations, in accordance with Eq. (A1). The vector $\vec{a}$ constituting the normalization condition, Eq. (23), takes the form

$$\vec{a}=\begin{bmatrix}\dfrac{1+k_p^*/q_0}{2}\\ \dfrac{1+k_c^*/q_0}{2}\left\{\dfrac{1}{D^{+*}(k_c)}-\dfrac{1}{D^{-*}(k_c)}\right\}\\ 0\end{bmatrix}. \tag{A6}$$

In the slab problem the matrix elements are analogous to Eq. (A3), the only difference being in the exponential factors coming from the coexistence of copropagating and contrapropagating waves, Eq. (27) (we do not show the expressions due to their obvious form). The vector appearing in the normalization condition for even and odd parts, Eqs. (23) and (29), has the form

$$\vec{a}_{e,o}=\begin{bmatrix}1+\dfrac{k_p^*}{q_0}+se^{ik_p^*L}\left(1-\dfrac{k_p^*}{q_0}\right)\\ \left\{1+\dfrac{k_c^*}{q_0}+se^{ik_c^*L}\left(1-\dfrac{k_c^*}{q_0}\right)\right\}\left\{\dfrac{1}{D^{+*}(k_c)}-\dfrac{1}{D^{-*}(k_c)}\right\}\\ 0\end{bmatrix}, \tag{A7}$$

and s is given by Eq. (26).

APPENDIX B: MATRIX ELEMENTS IN THE EXACT APPROACH: 1D CONTACT POTENTIAL

In this section we derive the matrix elements $V_{\sigma_1\sigma_2}$, Eq. (A3), within the model of the 1D contact electron-hole interaction,

$$\hat{H}_{\text{ex}}(z)=-\frac{\hbar^2}{2\mu}\frac{\partial^2}{\partial z^2}-\Omega\,\delta(z), \tag{B1}$$

where $\Omega=2a_B^*\text{Ry}^*$, a_B^* and $\text{Ry}^*=\hbar^2/(2\mu a_B^{*2})$ are, respectively, the exciton effective Bohr radius and Rydberg energy.

The exciton Green's function has the form

$$G(\varkappa;z)=\Omega^{-1}\frac{1}{\varkappa a_B^*-1}e^{-\varkappa|z|}, \tag{B2}$$

where $\varkappa$ is given by Eq. (10). The odd (non-S) eigenstates of the Hamiltonian, Eq. (B1), appear only in the continuum, having the wave functions

$$\varphi_\lambda(z)=2i\sin(\lambda z),\quad 0\leqslant\lambda<\infty, \tag{B3}$$

and the eigenenergies

$$\mathcal{E}_\lambda=\frac{\hbar^2\lambda^2}{2\mu}.$$

In half-space geometry, the matrix elements take the form

$$V_{00}(\varkappa_1,\varkappa_2)=\mathcal{M}^2\Omega^{-2}(\varkappa_1^* a_B^*-1)^{-1}\times(\varkappa_2 a_B^*-1)^{-1}U_{00}(\varkappa_1,\varkappa_2),$$

$$V_{01}(\varkappa_1,\varkappa_2)=\mathcal{M}\Omega^{-1}(\varkappa_1^* a_B^*-1)^{-1}[U_{01}(\varkappa_1,\varkappa_2)-U_{01}(\varkappa_1,-\varkappa_2)],$$

$$V_{11}(\varkappa_1,\varkappa_2)=U_{11}(\varkappa_1,\varkappa_2)-U_{11}(\varkappa_1,-\varkappa_2)-U_{11}(-\varkappa_1,\varkappa_2)+U_{11}(-\varkappa_1,-\varkappa_2), \tag{B4}$$

where

$$U_{\sigma_1\sigma_2}(\varkappa_1,\varkappa_2)=\frac{1}{\varkappa_1^*+\varkappa_2+i\beta_e(k_1^*-k_2)}+(-1)^{\sigma_1+\sigma_2}\frac{1}{\varkappa_1^*+\varkappa_2+i\beta_h(k_1^*-k_2)}, \tag{B5}$$

where k_i and $\varkappa_i$ are related to each other through Eq. (10) or (A4), $\beta_{e,h}=m_{e,h}/M$.

In slab geometry the matrix elements of $\hat{W}$ and $V_{\sigma_1\sigma_2}$ have the same form as defined in Eqs. (A2) and (B4), but $U_{\sigma_1\sigma_2}$ are different,

$$U_{\sigma_1\sigma_2}(\varkappa_1,\varkappa_2)=2[J_{\sigma_1\sigma_2}(\beta_e;\varkappa_1,\varkappa_2)+(-1)^{\sigma_1+\sigma_2}J_{\sigma_1\sigma_2}(\beta_h;\varkappa_1,\varkappa_2)], \tag{B6}$$

where

$$J_{\sigma_1\sigma_2}(\beta;\varkappa_1,\varkappa_2)=K(\beta;\varkappa_1,\varkappa_2,k_1,k_2)+(-1)^{\sigma_1+\sigma_2}\times e^{-i(k_1^*-k_2)L}K(\beta;\varkappa_1,\varkappa_2,-k_1,-k_2)+s[(-1)^{\sigma_1}e^{-ik_1^*L}K(\beta;\varkappa_1,\varkappa_2,-k_1,k_2)+(-1)^{\sigma_2}e^{ik_2L}K(\beta;\varkappa_1,\varkappa_2,k_1,-k_2)], \tag{B7}$$

$$K(\beta;\varkappa_1,\varkappa_2,k_1,k_2)=\frac{1-e^{-i[\varkappa_1^*+\varkappa_2+i\beta(k_1^*-k_2)]L}}{\varkappa_1^*+\varkappa_2+i\beta(k_1^*-k_2)}. \tag{B8}$$

Note that the factor of 2 appears in Eqs. (A7), (B6), and (29) due to artificial separation of the slab problem into even ($s=1$) and odd ($s=-1$) parts.

APPENDIX C: THEORY WITH MIXED ABC'S

In this section we derive the electric field in a semiconductor $0\leqslant Z\leqslant L$ (slab) or $Z\geqslant 0$ (half space), postulating mixed ABC's in generalized symmetric form

$$P_\nu'(0)=\alpha P_\nu(0),\qquad P_\nu'(L)=-\alpha P_\nu(L), \tag{C1}$$

where α is a state-independent complex parameter. Note that $\alpha=\infty$ yields Pekar's ABC's, considered in Sec. III, while $\alpha=0$ leads to TFB ABC's.

Following Kiselev *et al.*[8] we introduce the eigenvalue problem

$$u''(Z)+k^2u(Z)=0,\quad 0\leqslant Z\leqslant L, \tag{C2}$$

with the following BC's:

$$u'(0)=\alpha u(0),\qquad u'(L)=-\alpha u(L). \tag{C3}$$

A complete set of orthonormal functions

$$u_k(Z)=\frac{(\alpha+ik)e^{ikZ}-(\alpha-ik)e^{-ikZ}}{\sqrt{2[2\alpha+L(\alpha^2+k^2)]}} \tag{C4}$$

and discrete eigenvalues $k=k_\pm$, satisfying the dispersion equation

$$e^{ik_\pm L}=\pm\frac{\alpha-ik_\pm}{\alpha+ik_\pm},\quad k_\pm\geqslant 0, \tag{C5}$$

is the solution of the problem, Eqs. (C2) and (C3). Note that $\tilde{k}=-k$ also satisfies Eq. (C5) but corresponds to the same wave function $\tilde{u}(Z)=u^*(Z)=-u(Z)$, so we consider only $k\geqslant 0$.

Expanding $P_\nu(Z)$ into slab eigenmodes as in Eq. (36) and decomposing $E(Z)$ into homogeneous and inhomogeneous parts as in Eq. (37),

$$E(Z)=E^{\rm hom}(Z)+E^{\rm inh}(Z),$$

with

$$E^{\rm hom}(Z)=A_+e^{iq_1Z}+A_-e^{-iq_1Z},\qquad E^{\rm inh}(Z)=\sum_k E_k^{\rm inh}u_k(Z),$$

we arrive at Eqs. (38)–(40). The coefficients $A_\pm$ are found from the following set of equation [cf. with Eq. (41)]:

$$E(0)=A_++A_-+E^{\rm inh}(0),$$

$$E(L)=A_+e^{iq_1L}+A_-e^{-iq_1L}+E^{\rm inh}(L),$$

$$E'(0)=iq_1(A_+-A_-)+\alpha E^{\rm inh}(0),$$

$$E'(L)=iq_1(A_+e^{iq_1L}-A_-e^{-iq_1L})-\alpha E^{\rm inh}(L),$$

where we have used Eq. (C1). Excluding $E^{\rm inh}(0)$ and $E^{\rm inh}(L)$ we find

$$A_+=\frac{\chi_L(\alpha+iq_1)-\chi_0(\alpha-iq_1)e^{-iq_1L}}{(\alpha+iq_1)^2e^{iq_1L}-(\alpha-iq_1)^2e^{-iq_1L}},$$

$$A_-=\frac{\chi_0(\alpha+iq_1)e^{iq_1L}-\chi_L(\alpha-iq_1)}{(\alpha+iq_1)^2e^{iq_1L}-(\alpha-iq_1)^2e^{-iq_1L}},$$

where

$$\chi_0 = \alpha E(0) - E'(0),$$

$$\chi_L = \alpha E(L) + E'(L),$$

$$\chi_\pm = \chi_0 \mp \chi_L .$$

The electric field takes the form

$$E(Z) = A_+ e^{iq_1 Z} + A_- e^{-iq_1 Z} - \sum_{k_\pm} \chi_\pm \frac{ik_\pm}{q_1^2 - k_\pm^2} \frac{q_0^2 \varepsilon(k_\pm,\omega) - q_1^2}{q_0^2 \varepsilon(k_\pm,\omega) - k_\pm^2} \times \frac{(\alpha + ik_\pm) e^{ik_\pm Z}}{2\alpha + L(\alpha^2 + k_\pm^2)},$$

where we have extended $k_\pm$ to all possible values, both positive and negative [cf. with Eq. (C5)], using the antisymmetric form of u_k, Eq. (C4). $E^{\hom}(Z)$ can be also expanded into $u_k(Z)$ according to Eq. (40). Then,

$$E(Z) = \sum_{k_\pm} \chi_\pm \frac{ik_\pm}{q_0^2 \varepsilon(k_\pm,\omega) - k_\pm^2} \frac{(\alpha + ik_\pm) e^{ik_\pm Z}}{2\alpha + L(\alpha^2 + k_\pm^2)}. \tag{C6}$$

Note that in the special cases of Pekar's ($\alpha = \infty$) and TFB ($\alpha = 0$) ABC's, the expansion, Eq. (C6), is nothing else than the standard Fourier series, the eigenvalues having simple analytical form

$$\left.\begin{aligned} k_+ &= 0,\ \pm 2\frac{\pi}{L},\ \pm 4\frac{\pi}{L}, \ldots \\ k_- &= \pm\frac{\pi}{L},\ \pm 3\frac{\pi}{L}, \ldots \end{aligned}\right\} \quad \text{Pekar},$$

$$\left.\begin{aligned} k_+ &= \pm\frac{\pi}{L},\ \pm 3\frac{\pi}{L}, \ldots \\ k_- &= 0,\ \pm 2\frac{\pi}{L},\ \pm 4\frac{\pi}{L}, \ldots \end{aligned}\right\} \quad \text{TFB}.$$

The series in Eq. (C6) is well behaved everywhere $0 \leqslant Z \leqslant L$, for any finite α. However, its derivative has discontinuities at $Z = 0$ and $Z = L$ which show as divergent series. These peculiarities come from the fact that $E(Z)$ together with $E'(Z)$ satisfy some BC's other than those for the basic functions u_k, Eq. (C3). To remove these discontinuities we subtract from $E'(Z)$ the following term:

$$\sum_{k_\pm} \chi_\pm \frac{(\alpha + ik_\pm) e^{ik_\pm Z}}{2\alpha + L(\alpha^2 + k_\pm^2)},$$

which vanishes everywhere $0 < Z < L$ except two points on the boundaries,[33] where it has the same discontinuities as in Eq. (C6). After such a regularization we arrive at the series

$$E'(Z) = -\sum_{k_\pm} \chi_\pm \frac{q_0^2 \varepsilon(k_\pm,\omega)}{q_0^2 \varepsilon(k_\pm,\omega) - k_\pm^2} \frac{(\alpha + ik_\pm) e^{ik_\pm Z}}{2\alpha + L(\alpha^2 + k_\pm^2)}, \tag{C7}$$

which is now well behaved everywhere and can be used, together with Eq. (C6), for calculations of E and E' on the boundaries, necessary for Maxwell's BC's and evaluation of the reflectivity and transmission.

As soon as the slab is getting wider, the roots of the dispersion equation (C5) locate closer to the real axis, $k = \pi n/L$, with n integer, for any finite α. However, if $\mathrm{Re}(\alpha) < 0$, there are two "additional" roots near $k = \pm i\alpha$. Switching to integrals in Eqs. (C6) and (C7) and taking into account that $\chi_{L\to\infty} = 0$, we find for half-space geometry

$$E(Z) = \chi_0 \frac{i}{\pi} \int_{-\infty}^{\infty} dk \frac{k e^{ikZ}}{(\alpha - ik)[q_0^2 \varepsilon(k,\omega) - k^2]} + \chi_0 R(Z),$$

$$E'(Z) = -\chi_0 \frac{1}{\pi} \int_{-\infty}^{\infty} dk \frac{q_0^2 \varepsilon(k,\omega) e^{ikZ}}{(\alpha - ik)[q_0^2 \varepsilon(k,\omega) - k^2]} + \chi_0 R_1(Z),$$

where the terms R and R' are responsible for the additional roots,

$$R(Z) = R_1(Z) = 0, \quad \mathrm{Re}(\alpha) \geqslant 0,$$

$$\left.\begin{aligned} R(Z) &= \frac{2\alpha e^{\alpha Z}}{\alpha^2 + q_0^2 \varepsilon(i\alpha,\omega)} \\ R_1(Z) &= -\frac{2 q_0^2 \varepsilon(i\alpha,\omega) e^{\alpha Z}}{\alpha^2 + q_0^2 \varepsilon(i\alpha,\omega)} \end{aligned}\right\} \mathrm{Re}(\alpha) < 0.$$

*Email address: muljarov@gpi.ru

[1] S.I. Pekar, Zh. Éksp. Teor. Fiz. **33**, 1022 (1957) [Sov. Phys. JETP **6**, 785 (1958)].

[2] J.J. Hopfield, Phys. Rev. **112**, 1555 (1958).

[3] J.J. Hopfield and D.G. Thomas, Phys. Rev. **132**, 563 (1963).

[4] J.J. Sein, Phys. Lett. **32A**, 141 (1970); J.L. Birman and J.J. Sein, Phys. Rev. B **6**, 2482 (1972).

[5] R. Zeyher, J.L. Birman, and W. Brenig, Phys. Rev. B **6**, 4613 (1972).

[6] C.-S. Ting, M.J. Frankel, and J.L. Birman, Solid State Commun. **17**, 1285 (1975).

[7] V.A. Kiselev, B.S. Razbirin, and I.N. Uraltsev, Phys. Status Solidi B **72**, 161 (1975); I.V. Makarenko, I.N. Uraltsev, and V.A. Kiselev, *ibid.* **98**, 773 (1980).

[8] V.A. Kiselev, I.V. Makarenko, B.S. Razbirin, and I.N. Uraltsev, Fiz. Tverd. Tela (Leningrad) **19**, 1348 (1977) [Sov. Phys. Solid State **19**, 1374 (1977)].

[9] A. Stahl, Phys. Status Solidi B **94**, 221 (1979); I. Balslev and A. Stahl, *ibid.* **111**, 531 (1982); A. Stahl and I. Balslev, *ibid.* **113**, 583 (1982).

[10] A. Stahl and I. Balslev, *Electrodynamics of the Semiconductor*

Band Edge (Springer-Verlag, Berlin, 1987).
[11] A. D'Andrea and R. Del Sole, Phys. Rev. B **25**, 3714 (1982).
[12] A. D'Andrea and R. Del Sole, Phys. Rev. B **41**, 1413 (1990); K. Cho, A. D'Andrea, R. Del Sole, and H. Ishihara, J. Phys. Soc. Jpn. **55**, 1853 (1990).
[13] L. Gotthard, A. Stahl, and G. Czajkowski, J. Phys. C **17**, 4865 (1984).
[14] G. Czajkowski and P. Schillak, Phys. Status Solidi B **140**, 273 (1987).
[15] V.M. Axt and A. Stahl, Solid State Commun. **77**, 189 (1991).
[16] K. Victor, V.M. Axt, and A. Stahl, Z. Phys. B: Condens. Matter **92**, 35 (1993).
[17] A. Tredicucci, Y. Chen, F. Bassani, J. Massies, C. Deparis, and G. Neu, Phys. Rev. B **47**, 10 348 (1993).
[18] F. Bassani, G. Czajkowski, and A. Tredicucci, Z. Phys. B: Condens. Matter **98**, 39 (1995).
[19] Y. Chen, A. Tredicucci, and F. Bassani, Phys. Rev. B **52**, 1800 (1995).
[20] G. Czajkowski, F. Bassani, and A. Tredicucci, Phys. Rev. B **54**, 2035 (1996).
[21] K. Henneberger, Phys. Rev. Lett. **80**, 2889 (1998).
[22] D.F. Nelson and B. Chen, Phys. Rev. Lett. **83**, 1263 (1999); R. Zeyher, *ibid.* **83**, 1264 (1999); K. Henneberger, *ibid.* **83**, 1265 (1999).
[23] J. Tignon, T. Hasche, D.S. Chemla, H.C. Schneider, F. Jahnke, and S.W. Koch, Phys. Rev. Lett. **84**, 3382 (2000); H.C. Schneider, F. Jahnke, S.W. Koch, J. Tignon, T. Hasche, and D.S. Chemla, Phys. Rev. B **63**, 045202 (2001).
[24] G. Göger, M. Betz, A. Leitenstorfer, M. Bichler, W. Wegscheider, and G. Abstreiter, Phys. Rev. Lett. **84**, 5812 (2000).
[25] E. Muljarov and R. Zimmermann, in *Proceedings of the 25th ICPS*, Springer Proceedings in Physics, Vol. 87, edited by N. Miura and T. Ando (Springer, Berlin, 2001), p. 101.
[26] D. Viri and R. Del Sole, Phys. Rev. B **52**, 11 891 (1995).
[27] W.H. Press, S.A. Teukolsky, W.T. Vetterling, and B.P. Flannery, *Numerical Recipes in C* (University Press, Cambridge, England, 1992).
[28] A. D'Andrea and R. Del Sole, Phys. Rev. B **32**, 2337 (1985).
[29] S. Satpathy, Phys. Rev. B **28**, 4585 (1983).
[30] We define the excitonic polarization P in such a way that the induction of the electric field has the form $D=\varepsilon_b E+P$.
[31] Strictly speaking, the energy flux conservation law imposes the limitation $\mathrm{Im}(\alpha)=0$; see, e.g., M.F. Bishop and A.A. Maradudin, Phys. Rev. B **14**, 3384 (1976).
[32] The contribution of the scattering states to the Green's function is much more sharp in case of the Coulomb potential, due to the level thickening near the continuum onset.
[33] This property follows from the completeness of the set of the basic functions, $\Sigma_k u_k^*(Z)u_k(Z')=\delta(Z-Z')$.